

Efficient Numerical Modeling of the Magnetization Loss on a Helically Wound Superconducting Tape in a Ramped Magnetic Field

Yoichi Higashi and Yasunori Mawatari

Abstract—We investigate theoretically the dependence of magnetization loss of a helically wound superconducting tape on the round core radius R and the helical conductor pitch in a ramped magnetic field. Using the thin-sheet approximation, we identify the two-dimensional equation that describes Faraday's law of induction on a helical tape surface in the steady state. Based on the obtained basic equation, we simulate numerically the current streamlines and the power loss P per unit tape length on a helical tape. For $R \gtrsim w_0$ (where w_0 is the tape width), the simulated value of P saturates close to the loss power $\sim (2/\pi)P_{\text{flat}}$ (where P_{flat} is the loss power of a flat tape) for a loosely twisted tape. This is verified quantitatively by evaluating power loss analytically in the thin-filament limit of $w_0/R \rightarrow 0$. For $R \lesssim w_0$, upon thinning the round core, the helically wound tape behaves more like a cylindrical superconductor as verified by the formula in the cylinder limit of $w_0/R \rightarrow 2\pi$, and P decreases further from the value for a loosely twisted tape, reaching $\sim (2/\pi)^2 P_{\text{flat}}$.

Index Terms—helically wound superconducting tape, magnetization loss, ramped magnetic field, analytical and numerical modeling.

I. INTRODUCTION

A rare-earth barium copper oxide (ReBCO) $\text{YBa}_2\text{Cu}_3\text{O}_{7-\delta}$ coated conductor on round core (CORC) cable was proposed a decade ago [1] as a new concept for practical superconducting (SC) coated conductor cables. This has since been developed into a much thinner CORC *wire* with a round core diameter of a few millimeters [2], [3] by using an alloy substrate with a thickness of as little as 30 μm . Flexible deformation along the former has ever been demonstrated, although such deformation degrades the critical current to some extent [3]–[5]. Furthermore, the current technology for fabricating CORC wires achieves the shortest conductor pitch (less than 10 mm [3]) among all high-temperature superconductor (HTS) cable concepts. Therefore, CORC wires show promise as practical SC wires for applications such as the high-field magnets used in particle accelerators and magnetic resonance imaging (MRI) machines.

To date, there have been relatively few reports on magnetization and transport alternating current (AC) loss measurements of CORC cables or wires without striation [4], [6], [7]. A helically wound tape structure (i.e., a continuous inclination of the tape) has been reported to decrease the magnetization loss

because of the reduced average perpendicular field component penetrating the tape over a full pitch [4]. However, other measurements have been reported showing higher AC loss in a helically wound tape in the fully penetrated state than in a flat tape. This fact is attributed to the anisotropy of the critical current density J_c with respect to the applied field [6]; a helically wound tape has a higher J_c than that of a flat tape in a certain portion of the tape oriented parallel to the field. This also results in a sizable AC loss reduction relative to the loss in a flat tape at low field strength [6]. For a single-layer CORC cable in the fully penetrated state, using more tapes in a single layer decreases the AC loss proportionally [6]. Meanwhile, in the case of a multi-layered CORC cable in the fully penetrated state, the AC loss increases in proportion to the number of layers in the cable [6]. An effect of a copper tube former on the magnetization and transport AC losses has been reported: eddy current loss makes a large contribution to the total transport AC loss, and the magnetic shielding reduces the magnetization AC loss at low field strength [7].

Regarding simulation studies, numerical simulations of AC losses based on the thin-sheet approximation have been carried out, the focus being the spiraled multi-layer coated conductors used for SC power transmission cables [8], [9]. Another approach to determining the electromagnetic properties of a power transmission cable composed of helically wound SC tapes is based on electric-circuit theory using the Bean model [10]. A computational method was developed by transforming three-dimensional helicoidal structures into two-dimensional ones [11]. To simulate a CORC cable, the AC losses were simulated at first by a two-dimensional model neglecting the winding of the tapes [12]. Later, an improved simulation study of the magnetization losses in CORC cables was carried out using three-dimensional models based on the H formulation [7], [13]. Simulations with three-dimensional models using the T-A formulation have also been conducted to investigate the AC losses in CORC cables, twisted stacked-tape conductor cables, and double coaxial cables with various transport currents and background magnetic fields [14]. Comprehensive simulations of the magnetization losses of CORC cables wound from the SC tapes with and without striation have been reported recently based on a three-dimensional model using the T-A formulation [15].

However, an analytical approach to modeling the AC losses of a CORC wire is currently lacking, partly because of the rather complex wire structure, and therefore the theoretical limit of the AC loss reduction in a CORC wire remains

Y. Higashi and Y. Mawatari are with National Institute of Advanced Industrial Science and Technology (AIST), Tsukuba, Ibaraki, 305-8568 Japan (e-mail: y.higashi@aist.go.jp).

Manuscript received April 3, 2019; revised July 22, 2019; accepted August 13, 2019.

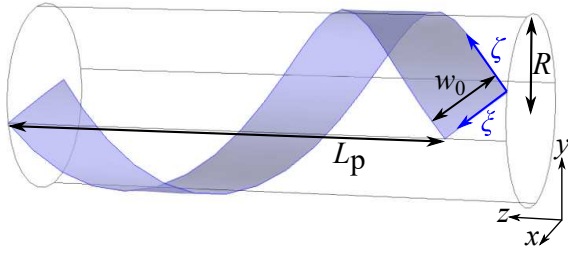


Fig. 1. Schematic of a helically wound superconducting (SC) tape of width w_0 and pitch L_p on a hollow cylinder of radius R . The axes (ξ, ζ) are on the tape surface.

elusive. Herein, we develop an analytical method for modeling the magnetization loss of a helically wound SC tape. The magnetization loss is simulated to obtain properties such as its dependences on R and L_p (see Fig. 1), and the simulation results are verified by the analytical formula in the limiting case of $w_0/R \rightarrow 2\pi$ or 0. We consider the situation in which ReBCO tapes wound round an MRI magnet are exposed to a magnetic field that is ramped up to high strength [16], [17]. The fully penetrated state is realized, resulting in the steady state in which the magnetic field profile on the tape is unchanged. Although the effects of tape stacking and J_c anisotropy on the AC losses are important issue [6] for the quantitative evaluation, we ignore such effects and focus instead on the simplest model. The presented models and results represent a first step toward further advanced research and development of a high-field magnet wound from CORC wires.

II. MODEL OF A HELICALLY WOUND SUPERCONDUCTING TAPE ON A HOLLOW CYLINDER

We consider a helically wound SC tape on a hollow cylinder as shown in Fig. 1. The tape width and thickness and the radius of the hollow cylinder are w_0 , d_0 , and R , respectively. The helically wound SC tape in the present simple model is assumed to be sufficiently thin ($d_0 \ll w_0$) that it can be approximated as a helical SC tape surface with infinitesimal thickness as depicted in Fig. 1. The SC tape surface is described by the coordinates (see Appendix A)

$$\begin{cases} x = R \cos[(k\zeta - \xi/R)/\sqrt{1 + (kR)^2}], \\ y = R \sin[(k\zeta - \xi/R)/\sqrt{1 + (kR)^2}], \\ z = (\zeta + kR\xi)/\sqrt{1 + (kR)^2}, \end{cases} \quad (1)$$

where $k = 2\pi/L_p$ and L_p is the pitch length of the helical conductor. The helically wound SC tape surface with a full pitch L_p corresponds to $-w_0/2 \leq \xi \leq w_0/2$ and $0 \leq \zeta \leq L_{\text{tape}}$, with $L_{\text{tape}} = L_p \sqrt{1 + (kR)^2}$ being the tape length corresponding to L_p . The ξ and ζ axes are orthogonal to each other on the helical SC tape surface as shown in Fig. 1.

III. RESPONSE TO AN APPLIED FIELD ON A HELICAL SUPERCONDUCTING TAPE

A. Reduced Faraday–Maxwell equation

We assume that the superconductor is in the steady state, which is plausible at high applied fields stronger than the full-

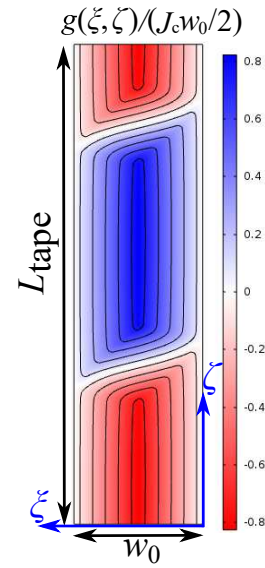


Fig. 2. Current streamlines and profile of the scalar function $g(\xi, \zeta)$ on a helically wound SC tape surface with $w_0 = 2$ mm and $L_p = 12$ mm for $\beta = 3$ mT/s and $R = 1.5$ mm. The tape length for one pitch of the helical conductor is $L_{\text{tape}} \approx 15.26$ mm.

flux-penetration field. We therefore neglect the contribution from the transport current because the magnetization losses are dominant over the transport losses at high field strength [18]. We also ignore the magnetic field due to the screening current because that field is much weaker than the applied field. In an applied field $\mathbf{B}_a(t) = B_a(t)\hat{x}$ that is ramped constantly at a rate $\beta = dB_a(t)/dt$, the Faraday–Maxwell equation in the steady state is

$$\nabla \times \mathbf{E} = -\frac{\partial \mathbf{B}}{\partial t} \approx -\frac{d\mathbf{B}_a(t)}{dt} = -\beta \hat{x}, \quad (2)$$

where \mathbf{E} (resp. \mathbf{B}) is the electric (resp. magnetic) field and \hat{x} is the unit vector in the x direction. With the thin-sheet approximation [19], we take account of only the response to the applied field component perpendicular to the tape surface. Consequently, the Faraday–Maxwell equation reduces to the following two-dimensional equation on the tape surface [20], [21] (see Appendix A):

$$\frac{\partial}{\partial \xi} \left(\rho_{\text{sc}} \frac{\partial g}{\partial \xi} \right) + \frac{\partial}{\partial \zeta} \left(\rho_{\text{sc}} \frac{\partial g}{\partial \zeta} \right) = \beta \cos \left(\frac{k\zeta - \xi/R}{\sqrt{1 + (kR)^2}} \right), \quad (3)$$

where $g(\xi, \zeta)$ a scalar function defined on the SC tape surface. The contour lines of $g(\xi, \zeta)$ describe the current streamlines on the tape surface, as depicted by the solid lines in Fig. 2. The SC property is incorporated through the electric field (\mathbf{E})–current density (\mathbf{J}) characteristics, namely $\mathbf{E} = \rho_{\text{sc}} \mathbf{J}$, with

$$\rho_{\text{sc}}(|\mathbf{J}|) = \frac{E_c}{J_c} \left(\frac{|\mathbf{J}|}{J_c} \right)^{n-1} \quad (4)$$

being the isotropic SC nonlinear resistivity. Herein, the electric field criterion is fixed to $E_c = 1$ $\mu\text{V}/\text{cm}$.

B. Boundary conditions

The specifications of the helically wound SC tape are summarized in Table I. We simulate the current streamlines and

TABLE I
 SPECIFICATIONS OF HELICALLY WOUND SC TAPE

Symbol	Quantity	Dimensions of helically wound SC tape
w_0	tape width	2 mm
d_0	tape thickness	2 μm
L_p	pitch length of helical conductor	2–200 mm
R	radius of hollow cylinder	$1/\pi$ –20 mm
		Superconducting characteristics
J_c	critical current density	5×10^{10} A/m ²
n	n -value	29

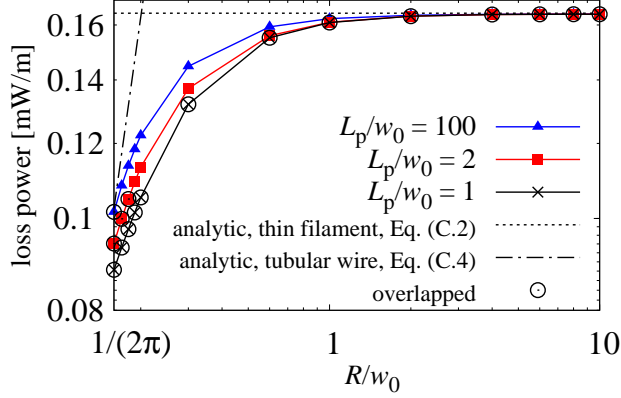


Fig. 3. Dependence of loss power per unit tape length on cylinder radius (plotted double logarithmically). The circles indicate where the SC tape overlaps.

the magnetization losses by solving Eq. (3) numerically using the commercial software COMSOL Multiphysics[®] [22]. The Dirichlet boundary condition $g(\xi = \pm w_0/2, \zeta) = 0$ is imposed on $g(\xi, \zeta)$ along the long edges of the SC tape, whereas the periodic boundary condition $g(\xi, \zeta) = g(\xi, \zeta + L_{\text{tape}})$ is imposed at the terminals of the SC tape with a full pitch. Herein, the field sweep rate is set to $\beta = 3$ mT/s because the typical field sweep rate of an MRI magnet is of the order of milliteslas per second [16], [17].

IV. RESULTS AND DISCUSSION

A. Current streamlines

By solving Eq. (3) numerically, the current density vector on the tape surface can be calculated via

$$\mathbf{J}(\xi, \zeta) = J_\xi \hat{\xi} + J_\zeta \hat{\zeta}, \quad J_\xi = -\frac{\partial g}{\partial \zeta}, \quad J_\zeta = \frac{\partial g}{\partial \xi}, \quad (5)$$

where $\hat{\xi}$ (resp. $\hat{\zeta}$) is the unit vector in the ξ (resp. ζ) direction. The color scale in Fig. 2 shows $g(\xi, \zeta)/(J_c w_0/2)$. The solid lines are the current streamlines, which are divided into two parts within a full pitch because of the helical winding, thereby reducing the effective tape length to $L_{\text{tape}}/2$.

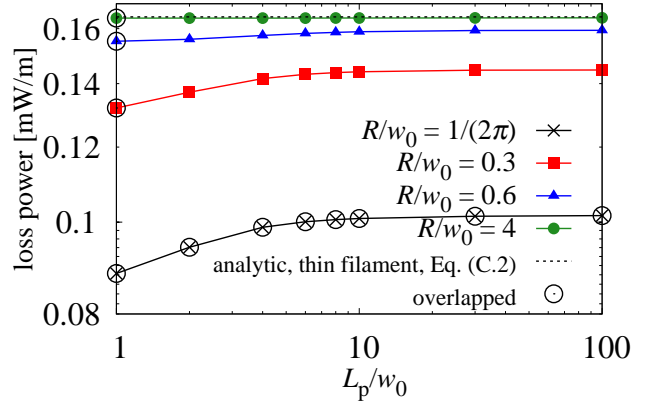
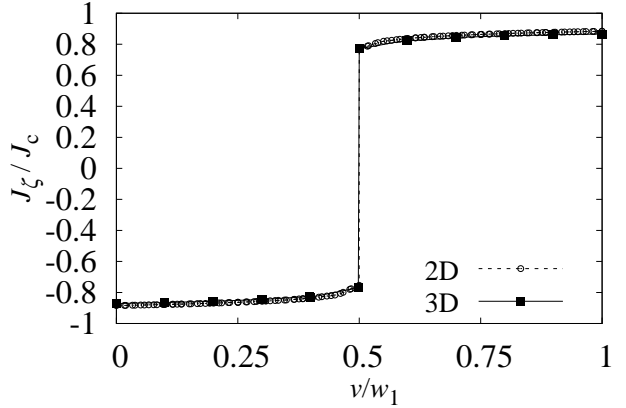


Fig. 4. Dependence of loss power per unit tape length on the pitch length of the helical conductor (plotted double logarithmically). The circles indicate where the SC tape overlaps.


 Fig. 5. Current density profile on a helical tape in the two and three dimensional models. The pitch length and the radius of the hollow cylinder are set to $L_p = 10w_0$ and $R = w_0$, respectively. The other parameters are common.

B. Magnetization loss

The loss power P per unit tape length is evaluated by (see Appendix B)

$$P = \frac{d_0}{L_{\text{tape}}} \int d\xi \int d\zeta \rho_{\text{sc}}(\xi, \zeta) \left[\left(\frac{\partial g}{\partial \xi} \right)^2 + \left(\frac{\partial g}{\partial \zeta} \right)^2 \right]. \quad (6)$$

Figure 3 shows the double logarithmic plot of the loss power per unit tape length versus R for different values of L_p . At $R/w_0 = 1/2\pi$, the helical SC tape overlaps with itself irrespective of L_p , and for $L_p/w_0 = 1$, the SC tape overlaps irrespective of R . The circles in Fig. 3 indicate where the tape overlaps.

For $R \gtrsim w_0$, the loss power saturates close to the analytically evaluated value (the dashed line in Fig. 3) in the thin-filament limit of $w_0/R \rightarrow 0$ via Eq. (C.2). For $n = 29$, Eq. (C.2) yields $P(w_0/R \rightarrow 0) \approx 0.165$ mW/m, which is close to $(2/\pi)P_{\text{flat}}$ (where P_{flat} is the loss power of the flat

tape) in the Bean limit of $n \rightarrow \infty$ as evidenced by a recent magnetization measurement [23] [see also Eq. (C.2)].

Meanwhile, for $R \lesssim w_0$, with decreasing R the loss power becomes much lower than that in the limit of $w_0/R \rightarrow 0$ (the dashed line in Fig. 3). Upon decreasing R/w_0 , the helically wound tape behaves more like a tubular wire, as discussed in Ref. [6]. Indeed, the loss power for $L_p/w_0 = 100$ at $R/w_0 = 1/2\pi$ shows quantitatively good agreement with the analytically evaluated loss power (the dashed-dotted line in Fig. 3) for a tubular wire via Eq. (C.4), although there is some deviation from the theoretical value for a tubular wire for $L_p/w_0 = 1$ and 2 because of the short pitch. The slope of the dashed-dotted line is two in the Bean limit because the loss power for a tubular superconductor increases with R^2 as in Eq. (C.5). The initial R slope for each value of L_p/w_0 is less than two, although it approaches two with increasing L_p/w_0 . We ascribe the initial slope being less than two to the finite pitch effect specific to the helically wound tape.

Figure 4 shows the dependence of the loss power per unit tape length on L_p in double logarithm form for different values of R . The loss power shows weak L_p dependence for $L_p/w_0 \lesssim 10$. At $R/w_0 = 4$, the loss power coincides with that evaluated via Eq. (C.2) in the thin-filament limit (the dashed line in Fig. 4) independent of L_p . Meanwhile, for $R/w_0 < 4$, the loss power becomes lower than the theoretical value in the thin-filament limit and becomes even lower with decreasing R as already mentioned in Fig. 3. The circles in Fig. 4 indicate where the tape overlaps.

Figure 5 shows the profiles of the current density $J_\zeta(v, \zeta = 0.5L_p)$ in the direction of the long dimension of a helical tape in two and three dimensional models. The profile of $J_\zeta(v, \zeta = 0.5L_p)$ on a helical tape shows a quantitative agreement between two and three dimensional models. Here, the axes v and ζ are defined via $(x, y, z) = (R \cos k(\zeta - v), R \sin k(\zeta - v), \zeta)$.

Next, we explain physically why the loss power decreases for $R \lesssim w_0$. The length scale for the penetration of magnetic flux vortices decreases as R decreases, thereby reducing the AC losses [24]. In the present study, we consider the steady state wherein the applied field should far exceed the full-flux-penetration field. We therefore consider that it is the reduced flux-penetration length scale, rather than the screening of the applied magnetic field, that reduces the loss power.

Next, we evaluate approximately the theoretically expected maximum reduction rate of the loss power upon reducing R . We evaluate the ratio of the loss power for $R/w_0 = 1/2\pi$ to that for $R/w_0 \gg 1$ (i.e., $w_0/R \rightarrow 0$) by using Eqs. (C.2) and (C.4):

$$\frac{P(w_0/R \rightarrow 2\pi)}{P(w_0/R \rightarrow 0)} = \frac{2 + 1/n}{\pi^{1+1/n}} \rightarrow \frac{2}{\pi} \quad (n \rightarrow \infty). \quad (7)$$

This suggests that by thinning the wire radius down to $R \ll w_0$, the loss power of the helical tape becomes smaller than P_{flat} by a factor of $(2/\pi)^2 \approx 0.405$ in accordance with a previous study [24]. Our numerical results confirm the reduction rate of the loss power. At $L_p/w_0 = 100$, the ratio of the loss power for $R/w_0 = 1/2\pi$ to that for $R/w_0 = 4$ is

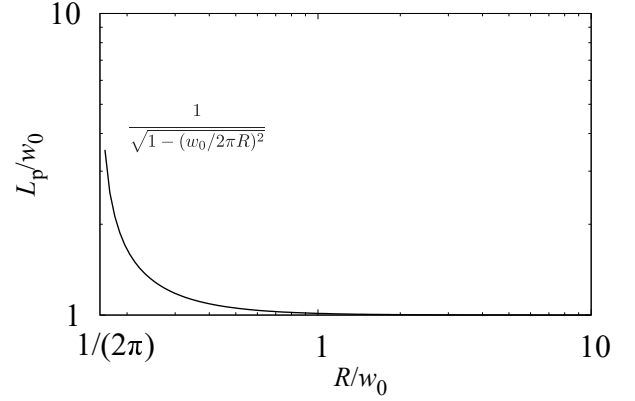


Fig. 6. Critical line on which the helically wound SC tape begins to overlap.

$P(R/w_0 = 1/2\pi)/P(R/w_0 = 4) \approx 0.619$, which agrees well with $(2 + 1/n)/\pi^{1+1/n} \approx 0.623$ [Eq. (7)] for $n = 29$.

Next, we consider the condition that must be met for the helically wound SC tape not to overlap. This is determined by $L_p > w_0/\cos \alpha$ (see Appendix A.1). By solving the condition with respect to L_p , we obtain the condition that $L_p > w_0/\sqrt{1 - (w_0/2\pi R)^2}$ (see Fig. 6).

C. CORC wire with multiple tapes

We discuss the effect of multiple tapes on magnetization losses in a single layer CORC wire. The response to an applied field is sufficiently large at high fields far above a full flux penetration field B_p that the interaction between SC tapes is relatively small and negligible, although the magnetic field shielding by neighboring tapes should be important to model a CORC wire wound by several tapes at low fields [6], [15]. The magnetic field due to the shielding current is of the order of $\mu_0 J_c d_0$ (≈ 0.126 T for the parameters adopted in this paper). It is sufficiently small comparing to the background field. Thus, we can ignore the contribution from a shielding current and treat total losses as a simple sum of the magnetization loss on an individual helical tape.

Our assumption should be plausible when the background field strength is as high as a few Tesla or at least above B_p . B_p for a single helical tape is approximately evaluated by the formula for a flat tape, $B_p = (\mu_0 J_c d_0 / \pi) [1 + \ln(w_0/d_0)] \approx 0.316$ T [25], where μ_0 is the magnetic permeability of a vacuum.

V. SUMMARY

We investigated theoretically the magnetization loss of a helically wound SC tape on a hollow cylinder in the steady state under a ramped field. For $R \gtrsim w_0$, the loss power saturates close to the value expected for a loosely twisted SC tape. Meanwhile, for $R \lesssim w_0$, it becomes lower than that value. Compared with the loss power P_{flat} for a flat SC tape, the loss power for a helical SC tape is roughly that for a loosely twisted tape ($\sim 2/\pi$ times lower than P_{flat}) for $R \gtrsim w_0$. Further reduction of the loss power value is expected by thinning the round core diameter down to $R \lesssim w_0$. For a thin wire with a radius of a few millimeters, the loss power per unit tape length is almost independent of L_p .

ACKNOWLEDGMENT

We would like to thank Y. Yoshida (AIST) for providing us with the properties and dimensions of commercial superconducting CORC[®] wires. We also thank R. Toyomoto (Kyoto Univ.) and N. Amemiya (Kyoto Univ.) for sharing unpublished AC-loss measurement and simulation data with us. The present work is based on the results obtained from a project commissioned by the New Energy and Industrial Technology Development Organization (NEDO).

APPENDIX A: DERIVATION OF REDUCED FARADAY–MAXWELL EQUATION

A.1. Model of helical tape

We use the following helical coordinates to model the helically wound SC tape:

$$\begin{cases} x = u \cos \theta, \\ y = u \sin \theta, \\ z = \theta/k + v, \end{cases} \quad (\text{A.1})$$

where $k = 2\pi/L_p$ and L_p is the pitch length of the helical conductor. The tape surface for one pitch length of the helical conductor corresponds to $u = R$, $0 \leq v \leq w_0/\cos \alpha$, and $0 \leq \theta \leq 2\pi$, where R is the radius of the hollow cylinder, w_0 is the tape width, and α is the lay angle defined by $\cos \alpha = kR/\sqrt{1+(kR)^2}$.

In general, the current density vector is described in terms of the current vector potential \mathbf{T} as $\mathbf{J} = \nabla \times \mathbf{T}$ so as to satisfy $\nabla \cdot \mathbf{J} = 0$. In the thin-sheet approximation, we regard the SC tape as a strip with infinitesimal thickness, and therefore the electric current flows on the tape surface at $u = R$. In this case, the current vector potential can be expressed in terms of the tape-normal unit vector ∇u as $\mathbf{T} = \nabla \times [g(\theta, v)\nabla u]$. Here, the scalar function $g(\theta, v)$ describes the current streamlines on the tape surface. The current density on the tape surface at $u = R$ is calculated as

$$\mathbf{J} = \nabla g(\theta, v) \times \nabla u = J_v \hat{\mathbf{v}} + J_\theta \hat{\boldsymbol{\theta}}, \quad (\text{A.2})$$

where $\hat{\mathbf{v}}$ and $\hat{\boldsymbol{\theta}}$ are the unit vectors in the v and θ directions, respectively, and

$$J_v = -\frac{1}{R} \frac{\partial g}{\partial \theta}, \quad J_\theta = \frac{\sqrt{1+(kR)^2}}{kR} \frac{\partial g}{\partial v}. \quad (\text{A.3})$$

A.2. Reduced Faraday–Maxwell equation on a helical tape

The electric field in the helical coordinates (A.1) is $\mathbf{E} = E_u \hat{\mathbf{u}} + E_v \hat{\mathbf{v}} + E_\theta \hat{\boldsymbol{\theta}}$ with

$$\hat{\mathbf{u}} = \nabla u = \hat{\mathbf{x}} \cos \theta + \hat{\mathbf{y}} \sin \theta, \quad (\text{A.4})$$

$$\hat{\mathbf{v}} = \nabla \theta/k + \nabla v = \hat{\mathbf{z}}, \quad (\text{A.5})$$

$$\begin{aligned} \hat{\boldsymbol{\theta}} &= (\sqrt{1+(ku)^2}/k)\nabla \theta + \nabla v/\sqrt{1+(ku)^2} \\ &= ku(-\hat{\mathbf{x}} \sin \theta + \hat{\mathbf{y}} \cos \theta + \hat{\mathbf{z}}/ku)/\sqrt{1+(ku)^2}. \end{aligned} \quad (\text{A.6})$$

Then, the electric field is expressed as $\mathbf{E} = E_u \nabla u + \tilde{E}_v \nabla v + \tilde{E}_\theta \nabla \theta$, where $\tilde{E}_v = E_v + E_\theta/\sqrt{1+(ku)^2}$ and $\tilde{E}_\theta = E_v/k + E_\theta\sqrt{1+(ku)^2}/k$. Using the relations $\nabla u \times$

$\nabla v = -(\sqrt{1+(ku)^2}/ku)\hat{\boldsymbol{\theta}}$, $\nabla v \times \nabla \theta = -\hat{\mathbf{u}}/u$, and $\nabla \theta \times \nabla u = -\hat{\mathbf{v}}/u$, we obtain

$$\begin{aligned} \nabla \times \mathbf{E} &= -\left(\frac{\partial \tilde{E}_v}{\partial u} - \frac{\partial E_u}{\partial v}\right) \frac{\sqrt{1+(ku)^2}}{ku} \hat{\boldsymbol{\theta}} \\ &\quad - \left(\frac{\partial \tilde{E}_\theta}{\partial v} - \frac{\partial \tilde{E}_v}{\partial \theta}\right) \frac{\hat{\mathbf{u}}}{u} - \left(\frac{\partial E_u}{\partial \theta} - \frac{\partial \tilde{E}_\theta}{\partial u}\right) \frac{\hat{\mathbf{v}}}{u}. \end{aligned} \quad (\text{A.7})$$

Because we adopt the thin-sheet approximation, we may consider the response to the perpendicular field component alone. Therefore, projecting Eq. (2) with eq. (A.7) onto the unit vector normal to the tape surface $\hat{\mathbf{u}}$ gives

$$\begin{aligned} \frac{\partial}{\partial v} \left(E_v/k + \sqrt{1+(ku)^2} E_\theta/k \right) \\ - \frac{1}{u} \frac{\partial}{\partial \theta} \left(E_v + E_\theta/\sqrt{1+(ku)^2} \right) = \beta \cos \theta \end{aligned} \quad (\text{A.8})$$

by using $\hat{\mathbf{u}} \cdot \hat{\boldsymbol{\theta}} = 0$ and $\hat{\mathbf{u}} \cdot \hat{\mathbf{v}} = 0$. Combining Eq. (A.8) with $(E_\theta, E_v) = \rho_{sc}(J_\theta, J_v)$, the Faraday–Maxwell equation on the tape surface $u = R$ is reduced to

$$\begin{aligned} \frac{\partial}{\partial v} \left[\rho_{sc} \frac{1+(kR)^2}{(kR)^2} \frac{\partial g}{\partial v} - \frac{\rho_{sc}}{kR} \frac{1}{R} \frac{\partial g}{\partial \theta} \right] \\ + \frac{1}{R} \frac{\partial}{\partial \theta} \left[\frac{\rho_{sc}}{R} \frac{\partial g}{\partial \theta} - \frac{\rho_{sc}}{kR} \frac{\partial g}{\partial v} \right] = \beta \cos \theta. \end{aligned} \quad (\text{A.9})$$

Although the derivation of the reduced Faraday–Maxwell equation (A.9) is clear in the coordinates of Eq. (A.1), Eq. (A.9) includes the divergent terms in the loosely wound limit of $kR \rightarrow 0$ as is obvious from geometric considerations. We therefore work in the coordinates in which the spatial axes (ξ, ζ) are orthogonal on the tape surface. An arbitrary position on the tape surface in the (ξ, ζ) coordinates is expressed in terms of (v, θ) as

$$\xi = v \cos \alpha, \quad \zeta = \sqrt{(R\theta)^2 + (\theta/k)^2} + v \sin \alpha, \quad (\text{A.10})$$

from which we have that

$$v = \frac{\sqrt{1+(kR)^2}}{kR} \xi, \quad \theta = \frac{k\zeta - \xi/R}{\sqrt{1+(kR)^2}}. \quad (\text{A.11})$$

Thus, on the tape surface $u = R$, from Eqs. (A.1) and (A.11), we obtain Eq. (1).

For $\mathbf{r} = x\hat{\mathbf{x}} + y\hat{\mathbf{y}} + z\hat{\mathbf{z}}$, we have that

$$\hat{\boldsymbol{\xi}} = \partial \mathbf{r} / \partial \xi = -\hat{\boldsymbol{\theta}}/ku + (\sqrt{1+(ku)^2}/ku)\hat{\mathbf{v}}, \quad (\text{A.12})$$

$$\hat{\boldsymbol{\zeta}} = \partial \mathbf{r} / \partial \zeta = \hat{\boldsymbol{\theta}}. \quad (\text{A.13})$$

Thus, we obtain

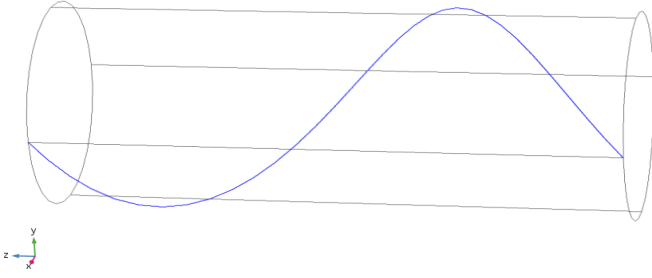
$$\hat{\mathbf{v}} = (\hat{\boldsymbol{\zeta}} + ku\hat{\boldsymbol{\xi}})/\sqrt{1+(ku)^2}, \quad \hat{\boldsymbol{\theta}} = \hat{\boldsymbol{\zeta}}. \quad (\text{A.14})$$

As for the reduced Faraday–Maxwell equation, substituting the expressions

$$\frac{1}{R} \frac{\partial g}{\partial \theta} = \frac{1}{R} \left(\frac{\partial g}{\partial \xi} \frac{\partial \xi}{\partial \theta} + \frac{\partial g}{\partial \zeta} \frac{\partial \zeta}{\partial \theta} \right) = \frac{\partial g}{\partial \zeta} \frac{1}{\cos \alpha}, \quad (\text{A.15})$$

$$\frac{\partial g}{\partial v} = \frac{\partial g}{\partial \xi} \frac{\partial \xi}{\partial v} + \frac{\partial g}{\partial \zeta} \frac{\partial \zeta}{\partial v} = \frac{\partial g}{\partial \xi} \cos \alpha + \frac{\partial g}{\partial \zeta} \sin \alpha \quad (\text{A.16})$$

into Eq. (A.9) yields Eq. (3). Furthermore, by substituting Eqs. (A.14)–(A.16) into Eq. (A.2), we have the screening current density Eq. (5) on the tape surface $u = R$.


 Fig. 7. Schematic of a helical tape in the thin-filament limit of $w_0/R \rightarrow 0$.

APPENDIX B: VECTORS IN (ξ, u, ζ) COORDINATES

First, by using Eq. (A.14), the coordinate transformation from the (θ, u, v) coordinates to the (ξ, u, ζ) ones can be achieved for an arbitrary vector $\mathbf{O} = (O_x, O_y, O_z)$. Second, in the same way, \mathbf{O} in the (ξ, u, ζ) coordinates is transformed to that in the (x, y, z) ones by using Eqs. (A.4)–(A.6), (A.12), and (A.13): $\mathbf{O} = O_u \hat{u} + O_v \hat{v} + O_\theta \hat{\theta} = O_u \hat{u} + O_\xi \hat{\xi} + O_\zeta \hat{\zeta} = O_x \hat{x} + O_y \hat{y} + O_z \hat{z}$, where $O_\xi \equiv kuO_v/\sqrt{1+(ku)^2}$ and $O_\zeta \equiv O_\theta + O_v/\sqrt{1+(ku)^2}$. In the case of the thin-sheet approximation, we have on the tape surface $u = R$ that

$$\begin{cases} O_x \approx (O_\xi \sin \alpha - O_\zeta \cos \alpha) \sin \theta, \\ O_y \approx -(O_\xi \sin \alpha + O_\zeta \cos \alpha) \cos \theta, \\ O_z \approx (O_\xi \cos \alpha + O_\zeta \sin \alpha). \end{cases} \quad (\text{B.1})$$

Herein, note that O_u vanishes in the thin-sheet approximation when \mathbf{O} refers to the current density or the electric field, neither of which has an out-of-plane component. Thus we have from Eq. (B.1) that $O_x^2 + O_y^2 + O_z^2 = O_\xi^2 + O_\zeta^2$. Note also that the Jacobian $\partial(x, y, z)/\partial(\xi, u, \zeta) = 1$.

APPENDIX C: MAGNETIZATION LOSS IN THIN-FILAMENT OR CYLINDER LIMIT

C.1. Thin-filament limit of $w_0/R \rightarrow 0$

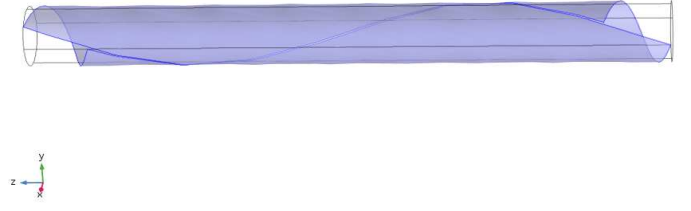
In the thin-filament limit, we may take the limit of $\xi/R \rightarrow 0$ while keeping kR finite (see Fig. 7). In this limit, the scalar function $g(\xi, \zeta)$ is almost uniform in the ζ direction, and therefore the second term on the left-hand side (l.h.s.) of Eq. (3) can be neglected because $\partial g/\partial \zeta \approx 0$. Thus, we obtain the equation for the scalar function:

$$\frac{\partial}{\partial \xi} \left(\rho_{\text{sc}} \frac{\partial g}{\partial \xi} \right) \approx \beta \cos \phi(\zeta), \quad (\text{C.1})$$

with $\phi(\zeta) = k\zeta/\sqrt{1+(kR)^2}$. Equation (C.1) has been solved previously with the Dirichlet boundary condition $g(\xi = \pm w_0/2, \zeta) = 0$ [20]. The loss power per unit tape length coincides with that for a twisted tape [20] and is readily evaluated as

$$\begin{aligned} P \left(\frac{w_0}{R} \rightarrow 0 \right) &= \frac{B\left(\frac{2n+1}{2n}, \frac{1}{2}\right)}{\pi} \left(\frac{\beta w_0}{2E_c} \right)^{\frac{1}{n}} \frac{J_c d_0 w_0^2 \beta}{2(2+1/n)} \\ &\rightarrow (2/\pi) J_c d_0 w_0^2 \beta / 4, \quad (n \rightarrow \infty), \end{aligned} \quad (\text{C.2})$$

where $B(p, q) = B(q, p) = 2 \int_0^{\pi/2} d\theta \cos^{2p-1} \theta \sin^{2q-1} \theta$ is the beta function and p and q are positive real numbers.


 Fig. 8. Schematic of a helical tape in the limit of $w_0/R \rightarrow 2\pi$. By taking the limit of $kR \rightarrow 0$ as well, a helical tape approaches to a gapped cylindrical superconductor.

C.2. Cylinder limit of $w_0/R \rightarrow 2\pi$

In the loosely wound limit of $L_p \rightarrow \infty$ (i.e., $kR \rightarrow 0$), $g(\xi, \zeta)$ can be viewed as uniform in the ζ direction, and thus the second term on the l.h.s. of Eq. (3) may be neglected. We note that $\theta = (k\zeta - \xi/R)/\sqrt{1+(kR)^2}$ on the right-hand side of Eq. (3) should be kept over a full pitch to take account of the helical winding effect of the tape. However, we encounter severe difficulty in evaluating the loss power analytically in this case. Instead, we take the cylinder limit of $w_0/R \rightarrow 2\pi$ in addition to the limit of $kR \rightarrow 0$ to understand the dependence of the loss power on R (see Fig. 8). By taking the limit of $kR \rightarrow 0$, we obtain

$$\frac{\partial}{\partial \xi} \left(\rho_{\text{sc}} \frac{\partial g}{\partial \xi} \right) \approx \beta \cos(-\xi/R). \quad (\text{C.3})$$

In this case, we can neglect the $kR\zeta$ term because it is not necessary to keep $\theta = (k\zeta - \xi/R)/\sqrt{1+(kR)^2}$ over a full pitch L_p in the limit of $w_0/R \rightarrow 2\pi$. Equation (C.3) lacks the information about the helical structure of the tape in the ζ direction and thus describes Faraday's law of induction in the steady state for an infinitely long gapped cylindrical superconductor. The loss power of a tubular superconductor per unit tape length is readily evaluated in the limit of $w_0/R \rightarrow 2\pi$ as

$$P \left(\frac{w_0}{R} \rightarrow 2\pi \right) = 2B \left(\frac{1}{2}, \frac{2n+1}{2n} \right) J_c d_0 R^2 \beta \left(\frac{\beta R}{E_c} \right)^{1/n}. \quad (\text{C.4})$$

Meanwhile, in the Bean limit of $n \rightarrow \infty$, the loss power of a gapped cylindrical superconductor per unit tape length is reduced to

$$\begin{aligned} P_{\text{gapped}} &= 2J_c d_0 \beta R^2 [1 - \cos(w_0/2R)] \\ &\begin{cases} \approx J_c d_0 w_0^2 \beta / 4 & (w_0/R \ll 1), \\ \rightarrow 4J_c d_0 R^2 \beta & (w_0/R \rightarrow 2\pi), \end{cases} \end{aligned} \quad (\text{C.5})$$

which coincide with the loss power for a flat tape in a swept field [20], [25] and a tubular superconductor (the R dependence is in accord with Ref. [24]), respectively.

REFERENCES

- [1] D. C. van der Laan, "YBa₂Cu₃O_{7- δ} coated conductor cabling for low ac-loss and high-field magnet applications," *Supercond. Sci. Technol.*, vol. 22, no. 6, p. 065013, 2009.
- [2] D. C. van der Laan, J. D. Weiss, P. Noyes, U. P. Trociewitz, A. Godeke, D. Abrahimov, and D. C. Larbalestier, "Record current density of 344 Amm⁻² at 4.2 K and 17 T in CORC[®] accelerator magnet cables," *Supercond. Sci. Technol.*, vol. 29, no. 5, p. 055009, 2016.

- [3] J. D. Weiss, T. Mulder, H. J. ten Kate, and D. C. van der Laan, "Introduction of CORC[®] wires: highly flexible, round high-temperature superconducting wires for magnet and power transmission applications," *Supercond. Sci. Technol.*, vol. 30, no. 1, p. 014002, 2016.
- [4] J. Šouc, M. Vojenčiak, and F. Gömöry, "Experimentally determined transport and magnetization ac losses of small cable models constructed from YBCO coated conductors," *Supercond. Sci. Technol.*, vol. 23, no. 4, p. 045029, 2010.
- [5] D. C. van der Laan, X. F. Lu, and L. F. Goodrich, "Compact GdBa₂Cu₃O_{7- δ} coated conductor cables for electric power transmission and magnet applications," *Supercond. Sci. Technol.*, vol. 24, no. 4, p. 042001, 2011.
- [6] M. Majoros, M. D. Sumption, E. W. Collings, and D. C. van der Laan, "Magnetization losses in superconducting YBCO conductor-on-round-core (CORC) cables," *Supercond. Sci. Technol.*, vol. 27, no. 12, p. 125008, 2014.
- [7] R. Terzioğlu, M. Vojenčiak, J. Sheng, F. Gömöry, T. F. Çavuş, and İ. Belenli, "AC loss characteristics of CORC[®] cable with a Cu former," *Supercond. Sci. Technol.*, vol. 30, no. 8, p. 085012, 2017.
- [8] K. Takeuchi, N. Amemiya, T. Nakamura, O. Maruyama, and T. Ohkuma, "Model for electromagnetic field analysis of superconducting power transmission cable comprising spiraled coated conductors," *Supercond. Sci. Technol.*, vol. 24, no. 8, p. 085014, 2011.
- [9] N. Amemiya, R. Nishino, K. Takeuchi, M. Nii, T. Nakamura, M. Yagi, and T. Okuma, "Ac loss analyses of superconducting power transmission cables considering their three-dimensional geometries," *Physica C: Superconductivity*, vol. 484, pp. 148 – 152, 2013.
- [10] T. Tominaka, "Current and field distributions of a superconducting power transmission cable composed of helical tape conductors," *Supercond. Sci. Technol.*, vol. 22, no. 12, p. 125025, 2009.
- [11] A. Stenvall, M. Siahraang, F. Grilli, and F. Sirois, "Computation of self-field hysteresis losses in conductors with helicoidal structure using a 2D finite element method," *Supercond. Sci. Technol.*, vol. 26, no. 4, p. 045011, 2013.
- [12] M. Solovyov, J. Šouc, and F. Gömöry, "AC loss properties of single-layer CORC cables," *J. Phys.: Conf. Ser.*, vol. 507, no. 2, p. 022034, 2014.
- [13] J. Sheng, M. Vojenčiak, R. Terzioğlu, L. Frolek, and F. Gömöry, "Numerical Study on Magnetization Characteristics of Superconducting Conductor on Round Core Cables," *IEEE Trans. Appl. Supercond.*, vol. 27, no. 4, pp. 1–5, 2017.
- [14] S. Fu, M. Qiu, J. Zhu, H. Zhang, J. Gong, X. Zhao, W. Yuan, and J. Guo, "Numerical Study on AC Loss Properties of HTS Cable Consisting of YBCO Coated Conductor for HTS Power Devices," *IEEE Trans. Appl. Supercond.*, vol. 28, no. 4, pp. 1–5, 2018.
- [15] Y. Wang, M. Zhang, F. Grilli, Z. Zhu, and W. Yuan, "Study of the magnetization loss of CORC[®] cables using a 3D T-A formulation," *Supercond. Sci. Technol.*, vol. 32, no. 2, p. 025003, 2019.
- [16] S. Yokoyama, J. Lee, T. Imura, T. Matsuda, R. Eguchi, T. Inoue, T. Nagahiro, H. Tanabe, S. Sato, A. Daikoku, T. Nakamura, Y. Shirai, D. Miyagi, and M. Tsuda, "Research and Development of the High Stable Magnetic Field ReBCO Coil System Fundamental Technology for MRI," *IEEE Trans. Appl. Supercond.*, vol. 27, no. 4, pp. 1–4, 2017.
- [17] T. Yachida, M. Yoshikawa, Y. Shirai, T. Matsuda, and S. Yokoyama, "Magnetic Field Stability Control of HTS-MRI Magnet by Use of Highly Stabilized Power Supply," *IEEE Trans. Appl. Supercond.*, vol. 27, no. 4, pp. 1–5, 2017.
- [18] K. Kajikawa, S. Awaji, and K. Watanabe, "Ac loss evaluation of an HTS insert for high field magnet cooled by cryocoolers," *Cryogenics*, vol. 80, pp. 215–220, 2016.
- [19] H. Zhang, M. Zhang, and W. Yuan, "An efficient 3D finite element method model based on the T–A formulation for superconducting coated conductors," *Supercond. Sci. Technol.*, vol. 30, no. 2, p. 024005, 2017.
- [20] Y. Higashi, H. Zhang, and Y. Mawatari, "Analysis of Magnetization Loss on a Twisted Superconducting Strip in a Constantly Ramped Magnetic Field," *IEEE Trans. Appl. Supercond.*, vol. 29, no. 1, pp. 1–7, 2019.
- [21] Y. Higashi and Y. Mawatari, "Electromagnetic coupling of twisted multifilament superconducting tapes in a ramped magnetic field," *Supercond. Sci. Technol.*, vol. 32, no. 5, p. 055010, 2019.
- [22] COMSOL Multiphysics[®]. [Online]. Available: www.comsol.com
- [23] C. S. Myers, M. D. Sumption, and E. W. Collings, "Magnetization and Flux Penetration of YBCO CORCTM Cable Segments at the Injection Fields of Accelerator Magnets," *IEEE Trans. Appl. Supercond.*, vol. 29, no. 5, pp. 1–5, 2019.
- [24] Y. Mawatari, "Superconducting tubular wires in transverse magnetic fields," *Phys. Rev. B*, vol. 83, p. 134512, 2011.
- [25] E. H. Brandt, "Superconductors of finite thickness in a perpendicular magnetic field: Strips and slabs," *Phys. Rev. B*, vol. 54, pp. 4246–4264, 1996.